Proceedings of the ASME 2011 Conference on Smart Materials, Adaptive Structures and Intelligent Systems
SMASIS2011
September 18-21, 2011, Scottsdale, Arizona, USA

SMASIS2011-5154

TIG WELDING OF NICKEL-TITANIUM TO 304 STAINLESS STEEL

Gordon Fox
Smart Vehicle Concepts Center
Department of Mechanical
and Aerospace Engineering
The Ohio State University
Columbus, Ohio 43210
Email: fox.483@osu.edu

Ryan Hahnlen
Smart Vehicle Concepts Center
Department of Mechanical
and Aerospace Engineering
The Ohio State University
Columbus, Ohio 43210
Email: hahnlen.1@osu.edu

Marcelo Dapino*
Smart Vehicle Concepts Center
Department of Mechanical
and Aerospace Engineering
The Ohio State University
Columbus, Ohio 43210
Email: dapino.1@osu.edu

ABSTRACT

Shape memory nickel-titanium (NiTi) is attractive for use in solid-state actuators as it exhibits large recoverable stresses, limited by its ultimate shear strength of over 120 ksi (960 MPa), and large recoverable strains, up to 8%. Broad application of NiTi is hindered by the expense, complexity, and lack of reliability in machining and joining it to structural materials. This paper investigates the use of orbital Tungsten Inert Gas (TIG) welding to join NiTi to 304 stainless steel (304 SS), a common structural material that can be readily machined and welded. Tubes of NiTi and 304 SS were joined using a nickel filler to mitigate the formation of brittle intermetallics. Both tubes had a 0.375 in (9.53 mm) outer diameter with wall thicknesses of 0.065 in and 0.075 in (1.7 mm and 1.9 mm) for the 304 SS and NiTi tubes, respectively. Viable joints were created and characterized through X-ray analysis, optical microscopy, hardness mapping, and strength testing. The joints had an average failure torque of 450 in-lb (52 N-m), corresponding to an ultimate shear strength of approximately 50 ksi (350 MPa). This was sufficient to detwin the NiTi in the tubes, which occurs at a shear stress of 16 ksi (110 MPa), and plastically deform the annealed 304 SS tubes. Optical microscopy and hardness mapping revealed a heat-affected zone 0.005 in ($125\ \mu m$*) wide with a maximum hardness of 817 HV. Outside of this heat-affected zone the hardness was not affected, indicating that no large-scale loss of superelastic or shape memory properties arises from TIG welding.*

INTRODUCTION

Shape memory alloys (SMAs) have the unique ability to undergo a reversible change in crystal structure when heated or cooled across their transition temperatures. With this transformation the stiffness of the alloy can be changed and large strains recovered. Shape memory Nitinol (NiTi) is attractive due to its relatively high stiffness, high blocking stress, large recoverable strain, and low cost compared to other SMAs. NiTi is utilized in medical devices such as stents and orthodontic wires due to these properties as well as its high bio-compatibility [1]. This alloy also holds promise in aerospace actuators because they have the potential to be simpler, smaller, and lighter than comparable electric or hydraulic actuation systems.

NiTi-based actuators have been successfully used on Boeing's Variable Geometry Chevron to bend a chevron on the trailing edge of a jet engine fairing into the exhaust stream. This improves the mixing characteristics of the boundary layer and reduces engine noise [2]. The small size, simplicity, and ruggedness of these actuators also makes them good candidates for actuators to be inserted into helicopter rotor blades to change their twist profile "on-the-fly" to optimize it for different flight conditions [3].

A major limitation on the use of NiTi is the difficulty of incorporating it into structures. Mechanical joining methods such as drilling bolt holes and threading NiTi rods are difficult and expensive because NiTi is very difficult to machine. Its high ductility inhibits chip breakage and causes heavy tool wear, and it is

*Address all correspondence to this author.

prone to chattering. Therefore, it can only be machined well under very narrow cutting conditions [4]. Adhesives can be used to join NiTi to other materials, but their strength is typically limited to several thousand psi (tens of MPa), they tend to degrade over time, and they are generally not biocompatable [5]. Soldering has been successfully accomplished either using aggressive fluxes [6] or ultrasonically vibrating soldering irons, but to obtain high strength joints, large contacting surface areas are required, which in turn constrain significant portions of the NiTi [7]. Welding holds the most promise for producing consistent, high-strength joints and welding NiTi to itself is now a relatively routine process. However, welding NiTi to dissimilar materials has proved more difficult [5]. It is desired to weld NiTi to ferrous alloys due to their low cost, high strength, good weldability, and machinability. An interlayer must be used to prevent the formation of brittle Ti-Fe intermetallics which severely degrade weld strength [8]. The heat produced can also degrade the shape-memory and superelastic properties of NiTi, which may only be partially recoverable through post-weld heat treatments and cold work [9]. Therefore, it is desirable to localize the heating of the NiTi being welded as much as possible.

This research investigates orbital Tungsten Inert Gas (TIG) welding for joints between NiTi and 304 stainless steel (304 SS) tubes using a nickel interlayer. TIG welding is a common industrial process for producing and repairing metal structures. Heat is applied to the base metals through an electric arc from a non-consumable tungsten electrode while shielding gas protects the weld from oxidation and atmospheric contamination. In orbital TIG welding, two round pieces are held together in a jig while the electrode orbits their circumference. It is an automated process, so parameters such as the speed of travel and the gap between the electrode and workpiece can be precisely controlled, resulting in consistent welds.

Tubes were used in this study to simulate the geometry of a torsional actuator. When a torque is applied, tubes have a more consistent shear stress across their cross section than solid rods, which aids analysis of the shear properties of these joints. Tubes also have a higher strength and stiffness-to-weight ratio than solid rods, which is especially important in aerospace applications where weight must be minimized. Three joints were created and characterized through X-ray analysis, optical microscopy, hardness mapping and mechanical strength testing. Von Mises equivalent stresses were calculated from the torsional strength of these joints to find the equivalent ultimate tensile strength of these joints. Additionally, a fourth joint was made for a torsional actuator to test integrating NiTi tubes into a mechanical system using these welds.

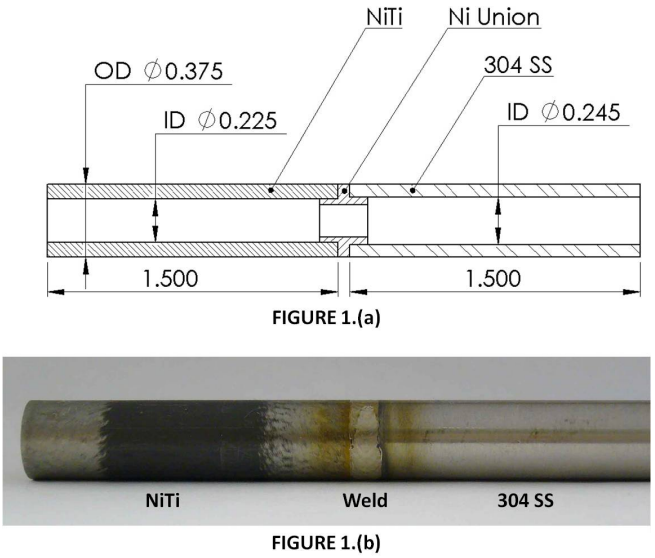

FIGURE 1. (a) DIAGRAM OF TIG WELD SPECIMEN (UNITS IN INCHES). (b) PHOTOGRAPH OF NiTi/304 SS TIG WELD SPECIMEN

EXPERIMENTAL METHODS

Sample Construction

NiTi and 304 SS tubes were welded together in a butt joint configuration. Both tubes have an outer diameter of 0.375 in (9.53 mm) and their inner diameters were left as-received: 0.225 in and 0.245 in (5.72 mm and 6.22 mm) for the NiTi and 304 SS tubes, respectively. This reduced the necessary pre-weld machining of the NiTi, which is both difficult and expensive. The three NiTi tubes for the characterization joints were cut via Electro-Discharge Machining (EDM). The tube for the actuator was cut with an abrasive saw and then faced on a manual lathe with hand-ground high-speed-steel bits. Chattering, excessive tool wear, and loss of shape-memory properties were not encountered in any of these machining processes. The nickel interlayers were placed with custom-made nickel unions inserted into the tubes prior to welding. Figure 1(a) shows a diagram of the weld joint and Fig. 1(b) shows a photograph of a completed joint.

The welds were made using an AMI M307 power supply coupled to a M9-750 weld head which was fitted with collets for 0.375 in OD tubes. Prior to welding, the oxide layer on the end of the outside of the NiTi tubes was removed with a tungsten carbide file. The oxide layer on the inside was removed with an inner diameter scraper.

Two different geometries of tungsten electrodes were used. For specimens 1 and 2 the electrode had a standard 22° included angle, while for specimens 3 and 4 it was 30°. Both electrodes had a 1/16 in (1.6 mm) diameter, 0.010 in (0.25 mm) wide flats, and used an arc gap of 0.045 in (1.1 mm). The duty cycles for the

primary and background electric pulses were 0.19, and the background current was 21.3 A. The primary current was reduced every 90° through the orbit from 70.8 A at the beginning to 53.1 A by the end to account for base metal heating. The welds were made in a single orbit which took approximately 20 seconds, with a 20 second pre and post-weld argon gas purge.

X-Ray Analysis

Prior to optical microscopy and mechanical testing, the first three welds were evaluated using a Kodak ACR 2000i Computed Radiography System. Because NiTi/ferrous alloy welds are very susceptible to cracking, this was done to ensure that no voids had formed due to weld contamination or large embedded cracks had developed due to intermetallic formation. The samples were inclined to provide an oblique viewing angle in the X-ray image.

Optical Microscopy and Hardness Mapping

The second specimen was sectioned via EDM and mounted for optical micrographs. The weld penetration and width of the optically observed heat affected zone (HAZ) were obtained from the micrographs using the imaging software ImageJ [10].

In addition to optically observing weld penetration and the HAZ, a hardness map was made from this specimen. The hardness map was created by making an array of indents with a diamond indenter and 100 gram load spaced 0.003 in (100 μm) apart in both the axial (X-axis) and radial (Y-axis) directions. The map was used to determine the hardness of the bulk NiTi tube as well as observe possible large scale HAZ formation. The resolution of this hardness map was not sufficient to investigate some small-scale features of the weld, so it was augmented with individual hardness tests which were conducted with a 10 gram load at points of interest.

Mechanical Testing

The first and third specimens were strength tested under a torsional load to failure. For fixturing purposes, 1/8 in (3.2 mm) diameter pin holes were drilled radially through each base metal, 0.6 in (15 mm) from the center of the weld. The torque was measured with a strain gauge based torque cell and the angular deflection between the sample grips was measured with an optical encoder. Deflection was applied at a rate of approximately 0.5 °/sec.

Similar mechanical tests were conducted on specimens made entirely out of NiTi and 304 SS to compare with the welded specimens' results. These specimens had the same geometry and fixturing as the welded specimens. Because the NiTi and 304 SS tubes had the same length as the TIG welded specimens, their measured deflections were halved to estimate how much each material contributed to the deflection of the TIG welded specimens.

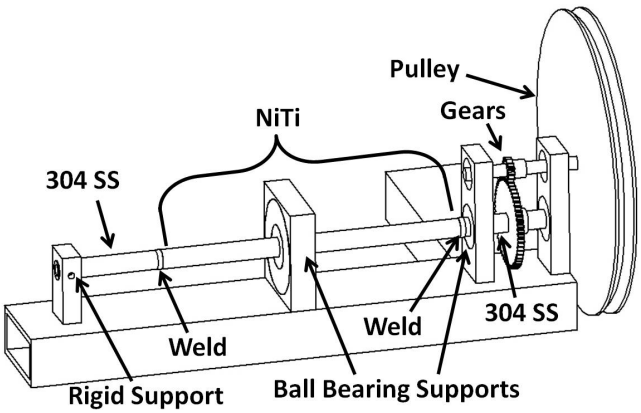

FIGURE 2. DRAWING OF TORSIONAL ACTUATOR.

System Integration

The fourth TIG welded specimen was used to build a torsional actuator to incorporate NiTi tubes into a mechanical system. The actuator has 304 SS tubes welded on both ends of a 6 in (150 mm) long NiTi tube. One of these 304 SS tubes is held rigidly while the one on the other end of the NiTi tube is supported with ball bearings to allow it to rotate freely. An additional ball bearing supports the middle of the NiTi tube to prevent torsional buckling. A gear is attached to the freely-rotating 304 SS tube which meshes with a smaller gear on a shaft connected to a pulley. A weight is suspended from a wire rope on this pulley, providing a torque to the NiTi tube. The NiTi tube was trained to have a two-way shape memory effect prior to welding, so it twists about 120° in one direction when heated and returns when cooled, regardless of whether a torque is applied to it. It is heated by an electrical resistance cartridge heater located inside of the tube and cooled by convection from an external fan. An illustration of this design is shown in Fig. 2.

RESULTS AND DISCUSSION

X-Ray Analysis

The completed samples showed no indications of cracking on the surface of the welds, however, it is possible that cracks had developed beneath the surface. X-ray images of specimens 1, 2, and 3 are shown in Fig. 3. These images do not indicate porosity or cracking in the welds, which would have appeared as dark regions. This suggests that the use of the nickel unions prevented large scale intermetallic formation and the orbital TIG process is suitable for creating viable structural joints between NiTi and 304 SS tubes.

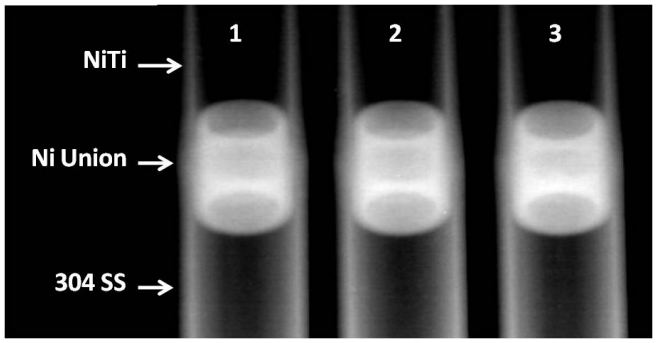

FIGURE 3. X-RAY IMAGE OF NiTi/304 SS TIG WELDS.

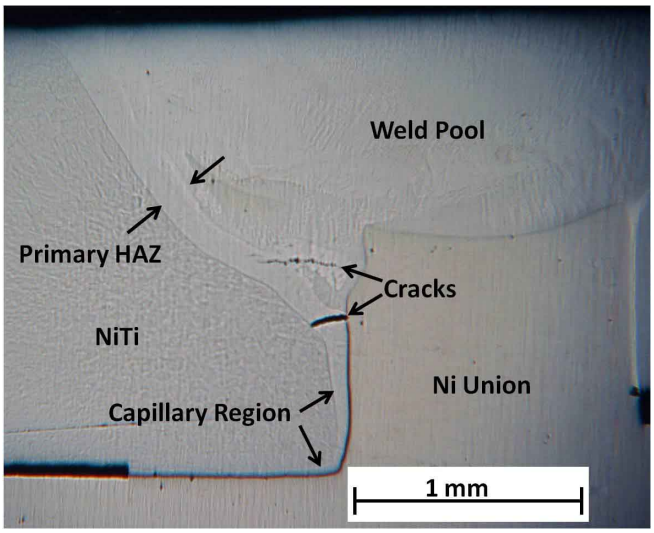

FIGURE 4. MICROGRAPH OF NiTi/304 SS WELD 2.

Optical Microscopy

A micrograph of specimen 2 is shown in Fig. 4. The weld penetrates through 0.052 in of the 0.075 in (1.3 mm of 1.9 mm) wall thickness of the NiTi tube. In between the weld pool and the NiTi at the left of the picture, a light shaded region is observed. This region is 0.005 in (125 μm) wide and follows the contour of the weld pool, then continues towards the center of the tube between the unmelted NiTi and nickel union. In this region, molten weld metal was likely drawn between the NiTi tube and nickel union through capillary action. There is a distinct boundary between this region and the rest of the weld pool and it is included in calculating the width of the HAZ. The region between the weld pool and NiTi tube was studied more in depth than the region between the weld pool and the 304 SS tube because that is where the welds failed during mechanical testing, and where defects in the weld were most likely to form.

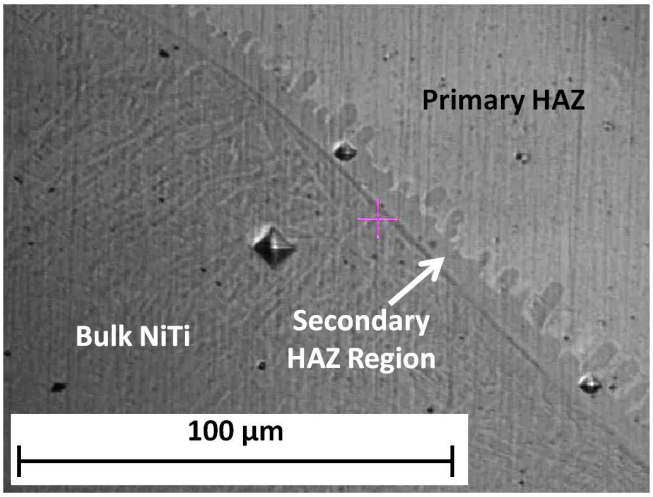

FIGURE 5. MICROGRAPH OF SECONDARY HAZ REGION OF NiTi/304 SS WELD 2.

Within the HAZ there is a secondary region which is shown in Fig. 5. This second region is very narrow and has an irregular boundary with the main HAZ. This region appears to consist of a homogeneous compound, and the irregular boundary with the main HAZ represents nucleation sites of this region.

It is assumed that loss of shape memory properties is limited to NiTi with increased hardness. Therefore, the narrow width of the optically observed HAZ indicates that there is little loss of the shape memory effect in the NiTi from recrystallization and loss of cold work due to heat generated in the welding process.

In the micrograph there are two instances of cracking that were not found in the X-ray images. Their absence from the X-ray analysis is likely due to two reasons: First, the top crack is relatively small and may not have been picked up due to the coarse focus of the X-ray system used. Second, both cracks are above the interface between the nickel union and NiTi tube which may have effectively hidden them in the X-ray image.

The cracks are located between the NiTi tube and the nickel union, so they are not attributed to the formation of Ti-Fe intermetallics. It is possible that another adverse compound formed due to the additional nickel. Further analysis is required to identify the elements present in the HAZ region. Because these defects were not observed in the X-ray image, it is unclear if similar defects were present in the mechanically tested samples. However, the uniformity of strength between the two mechanically tested samples shows that if such cracks were present, they did not cause much variation in the strength of the welds.

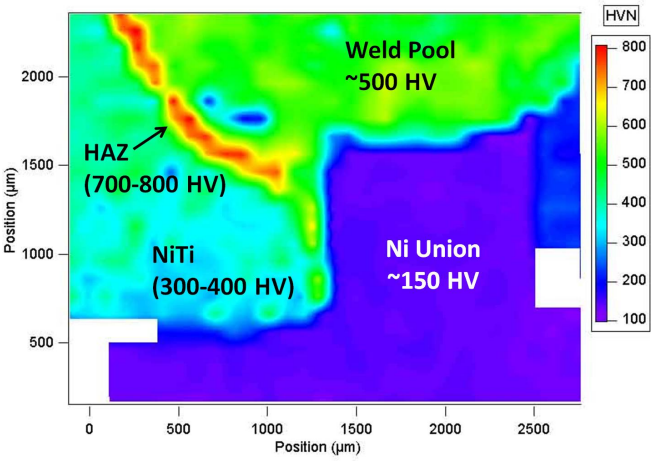

FIGURE 6. HARDNESS MAP OF NiTi/304SS WELD 2.

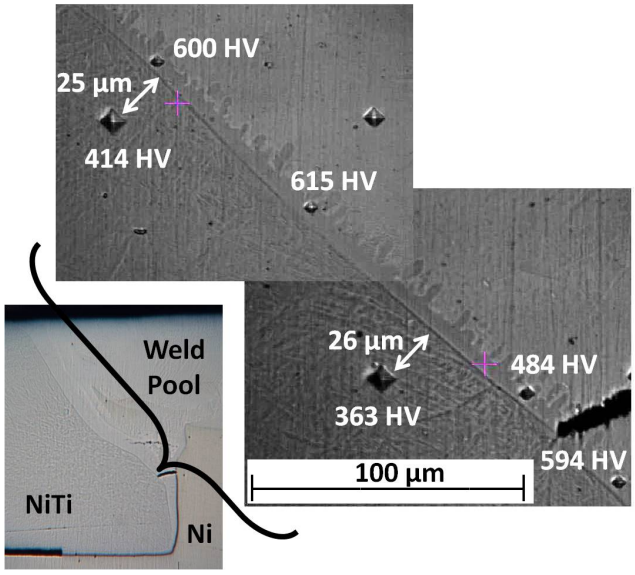

FIGURE 7. HARDNESS IN SECONDARY HAZ OF NiTi/304 SS WELD 2.

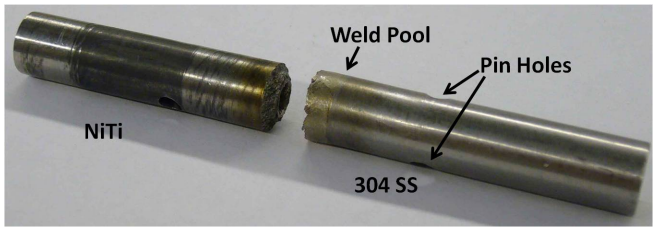

FIGURE 8. NiTi/304 SS WELD AFTER STRENGTH TESTING.

Hardness Mapping

The hardness map of specimen 2 is shown in Fig. 6. NiTi far from the weld pool has a hardness between 300–400 HV, which is typical for NiTi [11] and indicates that the thermo-mechanical properties have not been altered in this region. Along the weld boundary there is a region of increased hardness, up to 817 HV. This region corresponds to the lighter region observed in optical microscopy and indicates that the 0.005 in (125 μm) wide lighter region is the HAZ from the welding process.

Hardness measurements in the larger primary HAZ region were observed through the hardness map, but individual hardness tests were needed to measure the smaller secondary region because it is narrower than the space between indents in the hardness map. Figure 7 shows that this region has individual hardness values ranging from 484 to 615 HV, significantly harder than the bulk NiTi, but softer than the main HAZ region.

Two indents in the NiTi taken at 9.4 and 10.2×10^{-4} in (25 and 26 μm) from the HAZ boundary have hardness values of 414 and 363 HV, respectively. This indicates that at small distances from the optically observed HAZ, the material is similar to that of the bulk NiTi and supports the hypothesis that the optically observed boundary coincides with the HAZ as defined by the hardness measurements.

The resolution of the hardness map is also too large to provide information about the capillary regions observed between the unmelted NiTi and nickel union, so additional individual hardness data points were taken to investigate it. The hardness of the capillary region was found to range from 557 to 597 HV, which is harder than the bulk NiTi and similar to the hardness of the secondary HAZ region.

Through microscopy and hardness testing the identified HAZ was found to be small relative to both the thickness of the weld and overall tube length. Since the hardness of the NiTi piece returns to typical values for non-joined NiTi very close to the observed HAZ boundary, it is likely that any loss of cold work, shape memory, or superelastic properties is limited to the 0.005 in (125 μm) wide HAZ region. Orbital TIG welding has little effect on the properties of the bulk NiTi, and actuators using NiTi welded to 304 SS will have nearly the same properties as the NiTi in them before it was welded. This was also qualitatively confirmed in the mechanical tests by comparing the behavior of the TIG welded specimen with an unwelded NiTi tube.

Mechanical Testing

Specimens 1 and 3 were tested in torsion to failure, and broke at the interface between the weld pool and the NiTi tube, likely in the HAZ. Their breaking torques are listed in Tab. 1 and a photograph of a broken weld is shown in Fig. 8. The breaking torques were very consistent between the two samples, only differing by 2%, which indicates that this TIG welding process produces consistent joints.

TABLE 1. BREAKING TORQUES, CALCULATED SHEAR AND VON MISES STRENGTHS.

	Breaking	Shear Strength τ (ksi) [MPa]			Von Mises Tensile Strength σ_y (ksi) [MPa]		
	Torque	Case 1	Case 2	Case 3	Case 1	Case 2	Case 3
Spec.	(in-lb) [N-m]	Weld ID	NiTi ID	Ni ID	Weld ID	NiTi ID	Ni ID
1	458 [52.1]	60.8 [419]	50.8 [350]	46.0 [317]	105 [726]	88.0 [607]	79.7 [549]
2	448 [51.0]	59.5 [410]	49.7 [343]	45.0 [310]	103 [711]	86.1 [594]	77.9 [537]
Avg.	453 [51.6]	60.2 [415]	50.3 [347]	45.5 [314]	104 [719]	87.1 [601]	78.8 [543]

The maximum shear stress in the specimen is

$$\tau = \frac{T \times r}{J}, \tag{1}$$

where τ is the shear stress, T is the torque, r is the maximum radius, and J is the polar moment of inertia given by

$$J = \frac{\pi \times (OD^4 - ID^4)}{32}, \tag{2}$$

where OD and ID are the outer and inner diameters of the tube, respectively.

Since there is only partial weld penetration and a capillary region with unknown bonding properties, calculations of the shear stress in the joints are more difficult than for a homogeneous material. The material in this capillary region may act as a brazing joint, allowing stress transfer from the NiTi tube to the nickel union, or it may transmit no stress at all. To give a range of the strengths of the welds, maximum breaking shear stresses are calculated using three different assumptions. The first assumption is that this capillary region transmits no stress, so the ID used in Eqn. (2) is the ID of the bottom of the weld penetration, 0.271 in (6.88 mm). The second assumption is that it transmits stress directly through the butt end of the NiTi tube to the nickel union, so the ID used is that of the NiTi tube, 0.225 in (5.72 mm). The last assumption is that this region transmitted stress through the entire contacting area of the NiTi tube and nickel union, so the ID of the nickel union is used, 0.165 in (4.19 mm). These calculated ultimate shear stresses are tabulated in Tab. 1.

The von Mises equivalent stress can be calculated from the general stress tensor by

$$\sigma_y = \sqrt{\frac{(\sigma_{11}-\sigma_{22})^2 + (\sigma_{22}-\sigma_{33})^2 + (\sigma_{11}-\sigma_{33})^2 + 6(\sigma_{12}^2 + \sigma_{23}^2 + \sigma_{31}^2)}{2}}, \tag{3}$$

where σ_y is the von Mises equivalent stress. In the case of pure shear stress, such as torsion, the normal stresses are zero, $\sigma_{11} = \sigma_{22} = \sigma_{33} = 0$, and the out-of-plane shear stresses are zero, $\sigma_{23} = \sigma_{13} = 0$. This leaves only the in-plane shear stress: $\sigma_{12} = \tau$. With this, Eqn. (3) reduces to

$$\sigma_y = \tau\sqrt{3}, \tag{4}$$

where τ is the shear stress from Eqn. (1). The von Mises equivalent tensile strengths of the welds are listed in Tab. 1.

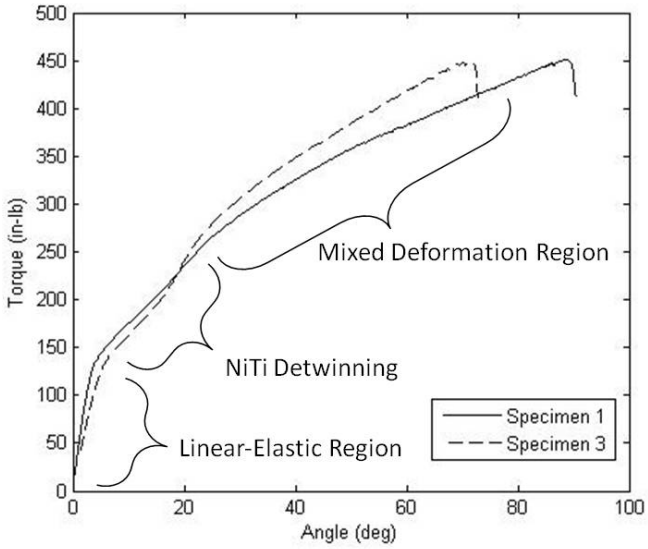

FIGURE 9. TORQUE VS. ANGLE FROM NiTi/304 SS WELD MECHANICAL TEST.

A plot of the torque as a function of the angle of twist of the specimen grips is shown in Fig. 9. There are three main regions: an initial linear-elastic region, the NiTi in the specimen detwinning, and a mixed deformation region which includes elastic deformation of the detwinned NiTi tube and plastic deformation of the 304 SS tube. Due to the thick walls of the specimens, the inner and outer fibers were at significantly different shear stresses at a given torque. This means that the onset of detwinning in the

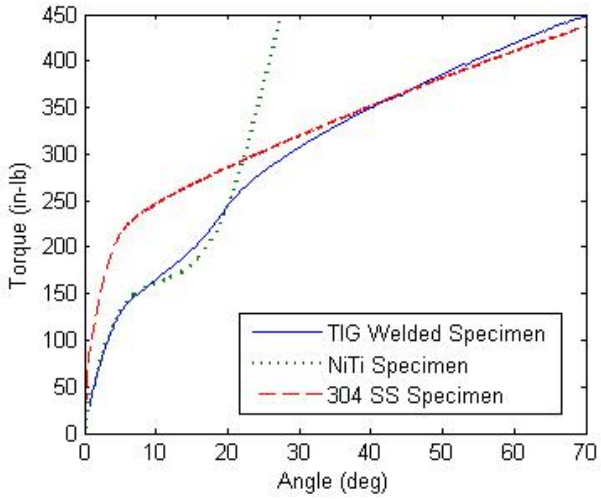

FIGURE 10. TORQUE VS. ANGLE OF WELDED SPECIMEN AND UNWELDED BASE METALS.

NiTi tube and yielding in the 304 SS tube occurs over a range of torques, which is unlike tension tests where each of these occur at a single load. This makes changes in the slope of the torque versus angle plot at the start of detwinning and yielding rounder and less defined than in plots of tensile load versus deformation.

The torque versus angle curve of the TIG welded specimens is compared to that of unwelded NiTi and 304 SS tubes in Fig. 10. This comparison helps identify the detwinning and plastic deformation regions in Fig. 9. The start of detwinning occurred at similar torques in the welded specimens and in the NiTi tube but the welded specimen required greater stress to continue detwinning, which correlates with the findings of Falvo et al. on laser welds of NiTi [11]. The onset of plastic deformation in the 304 SS tube around 230 in-lb (26.2 N-m) coincides with the torque where the deformation of the welded specimen started deviating significantly from that of the NiTi tube. Because the NiTi tube was stiffer after detwinning than the plastically deforming 304 SS tube, most of the deflection of the welded specimen in the mixed deformation region in Fig. 9 was due to yielding of the 304 SS tubes, not the NiTi tubes. Yielding was not encountered in the NiTi tubes before 450 in-lb (51.2 N-m), so it can be concluded the NiTi in the welded specimens did not yield before the welds failed.

From the plots of the welded specimens and NiTi tube, it can be seen that the initial linear region ends and detwinning starts at around 140 in-lb (15.9 N-m). This corresponds to a shear stress of 15.5 ksi (107 MPa) and a von Mises stress of 26.9 ksi (185 MPa) in the outer fibers of the NiTi tube.

The stainless steel used in this study was annealed, and the outer fibers started to yield at a torque of about 230 in-lb

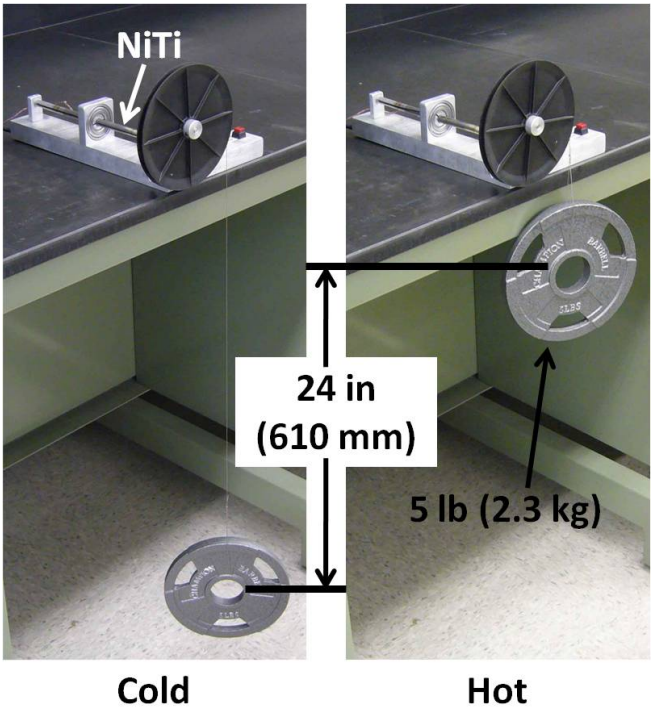

FIGURE 11. TORSIONAL ACTUATOR BEFORE AND AFTER HEATING.

(26.2 N-m), which was very close to the end of the detwinning region. This is undesirable for mechanisms using these welds because all the NiTi in them cannot be safely detwinned without starting to yield the 304 SS tubes connected to it. However, the strength of 304 SS tubes can be increased via heat treatment and cold work to be greater than the strength of these welds [12]. Changing the geometry of the 304 SS piece welded to the NiTi tubes cannot increase the strength of the joints much by itself. If solid rods were used instead of tubes, the strength found from Eqn. (1) only increases by 20%. This means that a solid 304 SS rod would start to yield at 275 in-lb (31.4 N-m), which is still not safely more than the torque necessary to detwin all of the NiTi tube.

System Integration

The actuator is able to successfully lift the weight when heated and lower it when cooled. Once the cartridge heater inside the NiTi tube is turned on, it takes about 30 seconds to heat it above the austenite finish temperature, then when it is turned off, about five minutes to cool back below its martensite finish temperature. The cooling process can be sped up with cooling water applied directly to the tubes.

The NiTi tube lifts the weight 24 in (610 mm) when actuated, which is shown in Fig. 11. The actuation of the NiTi tube

depends very little on the torque applied to it, so it lifts different weights the same distance. This is desirable for an actuator where the actuation distance must be consistent across a variety of loads.

The torque on the NiTi tube and welds can be calculated by

$$T = P \times r \times n, \tag{5}$$

where T is the torque, P is the weight, r is the pulley radius, and n is the gear ratio. For this actuator, P = 5 lb (2.3 kg), r = 3 in (76 mm) and n = 4, so the NiTi tube is subject to 60 in-lb (6.8 N-m) of torque. This is much less than the welds can withstand, but this torque is limited by the design of the 304 SS/gear attachment. With a different gear attachment design and geometry of the 304 SS, the full strength of these welds could be utilized and this actuator could lift up to 30 lb (14 kg).

CONCLUDING REMARKS

Successful TIG welds were made between NiTi and 304 SS tubes using a nickel interlayer. The joints' strengths were consistent between two mechanically tested specimens, which indicates that welds can be manufactured reliably using this process. The joints were strong enough to detwin the all of the NiTi in the tubes, which is desirable for its use in actuators. Yielding of the 304 SS tubes occurred before weld failure, so it cannot be used in its annealed state. But, with proper heat treatment and cold work, it can be made stronger than the welds. The shear strengths of the joints were in the range of 45-61 ksi (315–420 MPa), which correspond to von Mises equivalent stresses of 79–104 ksi (540–720 MPa).

Optical micrographs and a hardness map show a HAZ approximately 0.005 in (125 μm) wide, with hardnesses up to 817 HV. The NiTi outside of the HAZ shows no increase in hardness from its typical, unwelded value, so its superelastic or shape memory properties are likely not affected by the welding process. These are difficult to re-acquire through post weld heat treatments and cold work, so this simplifies the manufacturing process and means that welding does not degrade the torque and angle of twist available from a NiTi tube.

X-ray analysis revealed no large-scale cracks or voids in any of the three welds, which indicates that the nickel interlayer was successful in preventing the formation of brittle Ti-Fe intermetallics. Two small cracks were observed in the sectioned sample, though it is unclear if there were similar small cracks in the strength tested samples. Their consistent strengths indicate that even if there were cracks, they did not affect the weld strength much.

ACKNOWLEDGEMENTS

We would like to thank Jim Mabe and Tad Calkins of the Boeing Company for supplying the NiTi used in this study. We would like to thank the Edison Welding Institute for making the welds, particularly Steve Manring and Tim Frech. And, we would also like to thank Suresh Babu and Tapasvi Lolla for their assistance in collecting the hardness data.

REFERENCES

[1] Schetky, L., and Wu, M. "Issues in the Further Development of Nitinol Properties and Processing for Medical Device Applications".

[2] Hartl, D., Mooney, J., Lagoudas, D., Mabe, J., and Calkins, F., 2008. "Experimentally Validated Numerical Analysis of Aerostructures Incorporating Shape Memory Alloys". M. J. Dapino and Z. Ounaies, eds., Vol. **6929** of *Behavior and Mechanics of Multifunctional and Composite Materials*, SPIE.

[3] Mabe, J., Ruggeri, D. R., Rosenzweig, E., and Yu, C.-J. "NiTinol Performance Characterization and Rotary Actuator Design". E. H. Anderson, ed., Vol. **5388** of *Smart Structures and Materials 2004: Industrial and Commercial Applications of Smart Structures Technologies*.

[4] Weinert, K., and Petzoldt, V., 2004. "Machining of NiTi Based Shape Memory Alloys". *Materials Science and Engineering A,* ***378***, pp. 180–184.

[5] Hall, P., 1999. "Joining and Welding Nitinol".

[6] Hall, T., 1993. US Patent 5242759: Joint a Laminate and a Method of Preparing a Nickel-Titanium Alloy Member Surface for Bonding to Another Layer of Metal, September.

[7] Hahnlen, R., Fox, G., and Dapino, M., 2011. Joining of Shape Memory NiTi to Aluminum 2024 Using Ultrasonic Soldering. April.

[8] Hall, P., 2005. US Patent 6875949: Method of Welding Titanium and Titanium Based Alloys to Ferrous Metals, April.

[9] Wang, G., 1997. "Welding of Nitinol to Stainless Steel". In Proceedings of the International Conference on Shape Memory and Super Elastic Technologies, pp. 131–136.

[10] National Institutes of Health, U., 2009. ImageJ. http://rsbweb.nih.gov/ij/.

[11] Falvo, A., Furgiuele, F., and Maletta, C., 2005. "Laser Welding of a NiTi Alloy: Mechanical and Shape Memory Behaviour". *Materials Science and Engineering A,* ***412***, pp. 235–240.

[12] Mangonon, P., and Thomas, G., 1970. "Structure and Properties of Thermal-Mechanically Treated 304 Stainless Steel". *Metallurgical and Materials Transactions B,* ***1***(6), June, pp. 1587–1594.